DOI: 10.1002/ejic.200900169

Unconventional Spin Crossover in Dinuclear and Trinuclear Iron(III) Complexes with Cyanido and Metallacyanido Bridges

Ivan Šalitroš,[a] Roman Boča,*[a] L'ubor Dlháň,[a] Milan Gembický,[b] Jozef Kožíšek,[a] Jorge Linares,[c] Ján Moncol',[a] Ivan Nemec,[a] Lucia Perašínová,[a] Franz Renz,[d] Ingrid Svoboda,[e] and Hartmut Fuess[e]

Keywords: Iron / Structure elucidation / Schiff bases / Spin crossover / Exchange interactions

A nonsymmetrical triamine, 1,6-diamino-4-azahexane, was Schiff-condensed with (X-substituted) *o*-salicylaldehyde to yield pentadentate ligands X-L^5: salpet and MeBu-salpet. These ligands form mononuclear, dinuclear, and trinuclear Fe^{III} complexes, whose structures were determined by single-crystal X-ray analysis. Of the mononuclear complexes, [Fe^{III}(salpet)Cl] and [Fe^{III}(MeBu-salpet)Cl] are high spin (S = 5/2), whereas [Fe^{III}(salpet)CN]·MeOH is low spin (S = 1/2). The dinuclear and trinuclear complexes show a kind of thermally induced spin crossover. The dinuclear complex [L^5Fe^{III}(CN)$Fe^{III}L^5$](ClO_4)·2H_2O (L^5 = salpet) is a mixed-spin assembly: the *C*-coordinated Fe^{III} center is low spin (L) and the *N*-coordinated Fe^{III} center is high spin (H) at low temperature; an antiferromagnetic interaction occurs between them. This LH reference state is mixed with the LL one. Upon heating, the system shows an increasing content of the HH state. Also, the dinuclear complex [L^5Fe^{III}(CN)$Fe^{III}L^5$](BPh_4)·2MeCN (L^5 = MeBu-salpet) exhibits a spin transition between LH and HH spin pairs. The mixed-valence trinuclear complex [L^5Fe^{III}{Fe^{II}(CN)$_5$(NO)}$Fe^{III}L^5$]·0.5MeOH·3.75H_2O (L^5 = salpet) shows spin crossover with a residual high-spin fraction at liquid He temperature owing to the LL + LH ground state. The metallacyanido-bridged complex [L^5Fe^{III}{Ni(CN)$_4$}$Fe^{III}L^5$]·2MeOH (L^5 = MeBu-salpet) contains a high-spin pair, HH, over the whole temperature interval with a ferromagnetic exchange interaction. A theoretical model was outlined that allows simultaneous fitting of all available experimental data (magnetic susceptibility, magnetization, high-spin mole fraction obtained from the Mössbauer spectra) on a common set of parameters.

Introduction

The low-spin entity can be transformed into the high-spin species by heating when the energy gap ΔH is comparable to the thermal energy. The conversion L (low-spin) to H (high-spin) states is an entropy-driven unimolecular reaction ($\Delta S > 0$): there exists a critical temperature $T_c = \Delta H/\Delta S$ above which the conversion proceeds spontaneously. The degree of the conversion is characterized by the temperature dependence of the high-spin mole fraction, x_H, which defines the equilibrium constant $K = x_H/(1 - x_H)$; in an ideal case it follows the van't Hoff formula, that is, $\ln K$ vs. $1/T$ is a linear function.[1]

Spin crossover in mononuclear complexes is a case of electron bistability, associated with the existence of two minima (L and H) of the Gibbs energy. In dinuclear complexes, four distinct spin pairs can exist: LL, LH, HL, and HH (if intermediate spin states are ignored). It is not implied, however, that the LH pair is identical to the HL one. The corresponding energies of these electronic reference states are separated from the common origin by E_{LL}, E_{LH}, E_{HL}, and E_{HH} gaps, of which three are independent. Which energy order is actually followed is ruled by the crystal-field strength of the donor set (in general by the orbital angular momentum) and not by the spin angular momentum alone (Figure 1). Spin–spin interactions cause the formation of spin multiplets that are further split in the applied magnetic field and thus they dominate the magnetic behavior.

A floating nature of the reference energy levels, that is, the order of E_{LL}, E_{LH}, E_{HL}, and E_{HH}, was extensively modeled by DFT calculations.[2] It was found that in a series of structurally related dinuclear compounds [$(NCX)_2LFe^{II}$-bpym-$Fe^{II}L(NCX)_2$] the order of energy levels is: (a) HH, LL(222); (b) LH, HH(68), LL(137); (c) LL, LH(12),

[a] Institute of Inorganic Chemistry and Institute of Physical Chemistry, FCHPT, Slovak University of Technology, 81237 Bratislava, Slovakia
E-mail: roman.boca@stuba.sk
[b] Department of Chemistry, State University of New York at Buffalo, Buffalo, NY 14260, USA
[c] Groupe d'Etude de la Matière Condensée, CNRS-UMR 8635, University of Versailles, 78035 Versailles Cedex, France
[d] Institute of Inorganic Chemistry, Leibniz University, 30167 Hannover, Germany
[e] Material Sciences, Darmstadt University of Technology, 64287 Darmstadt, Germany
Supporting information for this article is available on the WWW under http://dx.doi.org/10.1002/ejic.200900169.

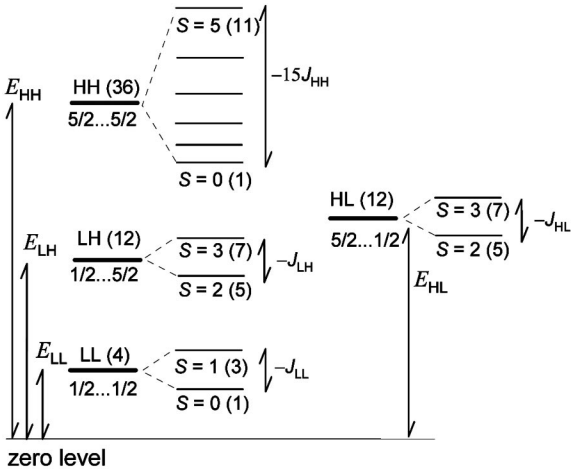

Figure 1. Reference states (LL, LH, HL, HH) and the corresponding spin multiplets (multiplicities in parentheses) for a dinuclear Fe^{III} system.

HH(20); (d) LL, LH(18), HH(24); and (e) LL, LH(47), HH(3); where the number in parenthesis is the energy of the state relative to the previous one (in $kJ\,mol^{-1}$). These studies proved that the common assumption that the LH state lies in between LL and HH is not always fulfilled.

When the energy gaps between the reference states are much higher than the exchange splitting, $E_{AB} >> |J_{AB}|$, these states are classified hereafter as well separated (class A, Figure 2). The exchange splitting is then a minor effect and the spin crossover could proceed abruptly. Notice, $E_{LL} < E_{LH} < E_{HH}$ needs be fulfilled in order to get the entropy of the spin transition positive ΔS[LL→LH] >0, ΔS[LH→HH] >0. Such a behavior is characteristic for the majority of dinuclear complexes showing spin crossover.[3]

When, for instance, $E_{HH} < E_{LL}$ holds true, the system stays high spin. However, at a high enough temperature ($kT > E_{LL} - E_{HH}$), the S-manifold of the LL state starts be populated, which can reflect itself in the Mössbauer spectra (MS) and the magnetic susceptibility.[4] Such an "*anti* spin crossover" case resembles the situation met in low-symmetry mononuclear Fe^{III} complexes in which the excited $^4A_{2g}$ ($\Gamma_7 + \Gamma_6$) term is admixed to the ground $^6A_{1g}$ ($\Gamma_6 + \Gamma_7 + \Gamma_7$) term.[5]

Rather complex situations appear when, on the contrary, the exchange splitting is comparable in energy with the separation of the reference states (class B, Figure 2). In such a case the subbands formed of S-multiplets can interfere. Group B/LL systems can exhibit spin crossover; owing to the thermally accessible high-spin multiplets, these systems can show a "residual high-spin mole fraction" in their MS even at liquid-helium temperatures. Spin crossover will proceed very gradually. Group B/HH stays high spin, but near room temperature an admixture from the LL pairs could be detected by MS.

The situation becomes even more complex because of the presence of the LH state, and one cannot exclude from consideration the intermediate spin states IL, II, and IH for low-symmetry coordination polyhedra. Moreover, the exchange coupling could be either antiferromagnetic or ferromagnetic, giving rise to multiplet reversal. Even trickier is the effect of the spin-orbit splitting, which makes the actual situation really complex. The spin–orbit coupling for a single Fe^{III} center splits the low-spin crystal-field term $^2T_{2g}$ into a pair of Γ_7 and Γ_8 multiplets [the splitting is $(3/2)\lambda = (3/2)\xi = 690\ cm^{-1}$]. Thus, for a single reference LL state we arrive at four substates: bonding (Γ_7-Γ_7), (Γ_8-Γ_8) and antibonding (Γ_7-Γ_7)*, (Γ_8-Γ_8)*. Clearly, such a model lies beyond the spin Hamiltonian formalism and has not been applied so far.

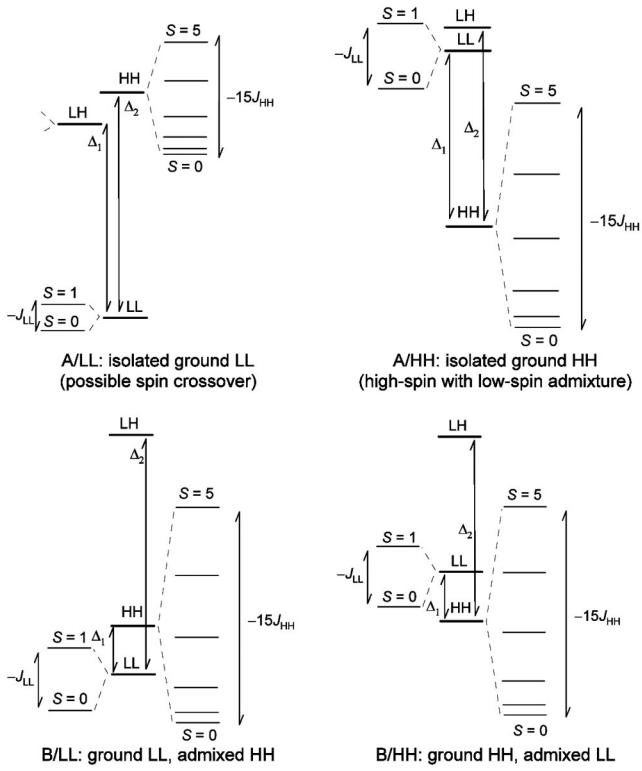

Figure 2. Basic classes of the dinuclear Fe^{III} complexes.

A usual assumption in literature is that the LH state (equivalent to the HL one) is positioned in between the LL and HH states. We met an unprecedented, unsymmetrical situation for the Fe–C–N–Fe unit, when the LH state is close to the ground LL state but its counterpart HL is not populated until room temperature.

A series of mononuclear precursors [FeL^5X] containing the Schiff-base pentadentate ligands L^5 was prepared. These were combined with a cyanido bridge to form binuclear complexes [$L^5Fe(CN)FeL^5$] that show a kind of spin crossover. A combination with metallacyanides results in the trinuclear species [$L^5Fe\{M(CN)_n\}FeL^5$].

Results and Discussion

Structure of Complexes

The molecular structure for three mononuclear Fe^{III} complexes is shown in Figure 3. These complexes are hexa-

coordinate with the coordination polyhedron deviating considerably from an octahedral shape. The chromophore resembles a *mer*-{FeN_3O_2X} configuration: the N-donor atoms of the former triamine and one oxygen atom of the former hydroxy group form an equatorial plane.

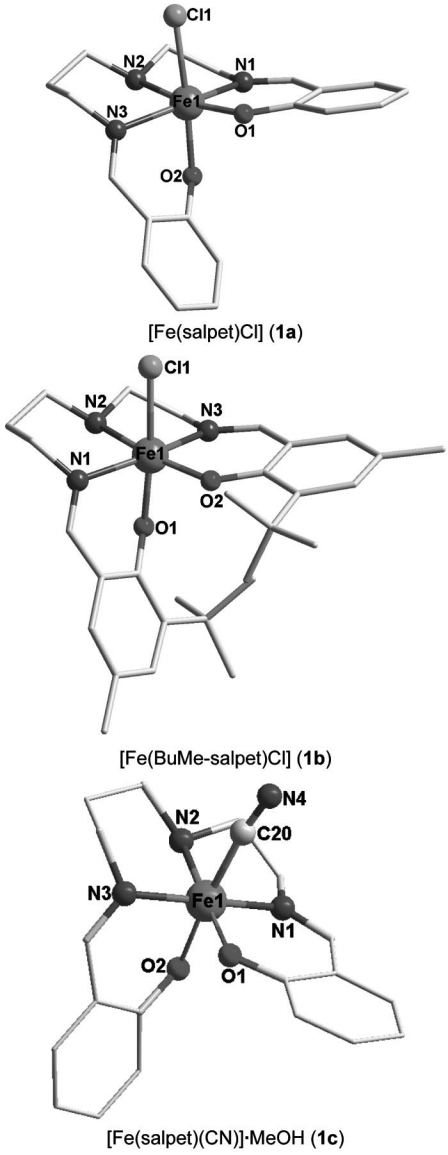

Figure 3. Molecular structure of mononuclear complexes (hydrogen atoms omitted for clarity). Selected bond lengths [Å] and out-of-plane angles [°] for **1a**: Fe1–N1 2.100, Fe1–N2 2.221, Fe1–N3 2.120, Fe1–O1 1.916, Fe1–O2 1.971, Fe1–Cl1 2.396; O2–Fe1–Cl1 175.47. For **1b**: Fe1–N1 2.093, Fe1–N2 2.198, Fe1–N3 2.093, Fe1–O1 1.969, Fe1–O2 1.897, Fe1–Cl1 2.409; O1–Fe1–Cl1 175.58. For **1c**: Fe1–N1 1.904, Fe1–N2 2.000, Fe1–N3 1.940, Fe1–O1 1.873, Fe1–O2 1.887, Fe1–C20 1.962 C20–N4 1.144; O2–Fe1–C20 174.89, Fe–C20–N4 172.76.

The distorted tetragonal bipyramid is completed by the second oxygen atom and the small ligand (X = Cl^- or CN^-). The out-of plane linkage O–Fe–X is close to the linear arrangement.

The bond lengths in **1a** (e.g., Fe–O 1.916, 1.971 Å) and **1b** (Fe–O 1.969, 1.879 Å) are, on average, much longer than the corresponding ones in **1c** (Fe–O 1.873, 1.887 Å). This indicates that **1a** and **1b** are high spin, whereas **1c** is low spin at the temperature of the experiment (T = 293 K). For complexes **1a** and **1b** a number of analogous structures [$Fe^{III}L^5Cl$] can be retrieved from the crystallographic data (L^5 stands for a pentadentate ligand) and all these complexes are high spin.[6] Complex **1c** belongs to a rare class of monocyanidoiron complexes structurally characterized so far. The CN group is coordinated in a linear manner (Fe1–C20–N4 172.76°) with a typical bond length (C20–N4 1.144 Å) of a triple bond.

The molecular structure of dinuclear complex **2a** is shown in Figure 4. The *mer*-{FeN_3O_2X} configuration found for the mononuclear precursor is maintained. The C-donor atom of the cyanide group coordinates to the first Fe^{III} center, and the corresponding contact (Fe1–C20 1.998 Å) is a bit longer relative to mononuclear precursor **1c** (1.962 Å). The CN group maintains the bond length typical for a triple bond (1.132 Å), and it is coordinated in a nearly linear manner (Fe1–C20–N4 172.52°; Fe2–N4–C20 173.44°). Its N-donor atom possesses a much longer contact to the second central atom (N4–Fe2 2.133 Å). The Fe1–N contacts are generally shorter (1.929, 2.032, 1.983 Å) than the Fe2–N(amine) ones (2.047, 2.139, 2.044 Å); this could indicate that the first Fe^{III} center is low spin, whereas the second Fe^{III} center is high spin at room temperature. The distances to the apical oxygen atoms are Fe1–O2 1.915 Å and Fe2–O3 1.938 Å, as compared to the mononuclear ones: Fe1–O2 1.971 Å, Fe1–O1 1.969 Å, and Fe1–O2 1.887 Å for **1a**, **1b**, and **1c**, respectively. Thus, they span the interval in between the pure low-spin and high-spin state.

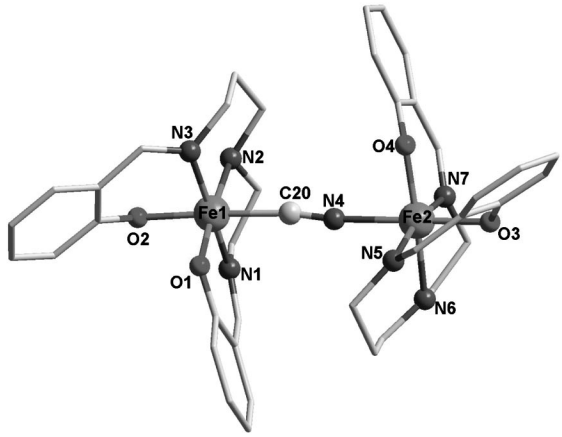

Figure 4. Molecular structure of the dinuclear complex [(salpet)-Fe(CN)Fe(salpet)]ClO_4·$2H_2O$ (hydrogen atoms, perchlorate anion, and solvent molecules omitted for clarity). Selected bond lengths [Å] for **2a**: Fe1–O1 1.877, Fe1–O2 1.915, Fe1–N1 1.929, Fe1–N2 2.032, Fe1–N3 1.983, Fe1–C20 1.998, C20–N4 1.132, Fe2–N4 2.133, Fe2–N5 2.047, Fe2–N6 2.139, Fe2–N7 2.044, Fe2–O3 1.938, Fe2–O4 1.902, Fe1–Fe2 5.256.

The molecular structure (90 K) for dinuclear complex **2b** is displayed in Figure 5. The cyanide group is disordered owing to the presence of the inversion center just in between

the iron atoms. The bridge is almost linear (the bond angles are 176.8, 176.8, 179.1, and 178.2°). The Fe1–O2 distance is short (1.889 Å), showing predominantly a low-spin character of the iron centers. The Fe–C and Fe–N bond lengths to the cyanide ligand are 1.867 and 2.177 Å, respectively. The averaged distances Fe–O(av.) 1.892 Å and Fe–N(av.) 2.011 Å at T = 90 K lie in between the pure low-spin and high-spin range.

The molecular structure of trinuclear complex **3a** is viewed in Figure 6. The peripheral Fe^{III} centers are Fe–NC coordinated at the distances characteristic for high-spin complexes (Fe1–N4 2.151 Å; Fe3–N9 2.193 Å); also, the other Fe–N(amine) contacts are rather long (Fe1–N 2.118, 2.199, 2.101 Å; Fe3–N 2.117, 2.209, 2.122 Å). The N–C bond lengths adopt characteristic values (1.142 and 1.137 Å) and are a bit bent coordinated (Fe1–N4–C20 160.02°; Fe3–N9–C21 157.96°). The nitrosyl group is linearly coordinated to the very central Fe^{II} atom at a short contact (Fe2–N5 1.688 Å; N5–O3 1.153 Å; Fe2–N5–O3 178.30°).

The molecular structure of trinuclear complex **3b** is shown in Figure 7. The complex is centrosymmetric, and according to metal–ligand distances it is high spin at room temperature: Fe–O 1.916, 1.901 Å and Fe–N 2.098, 2.239, 2.082, 2.158 Å.

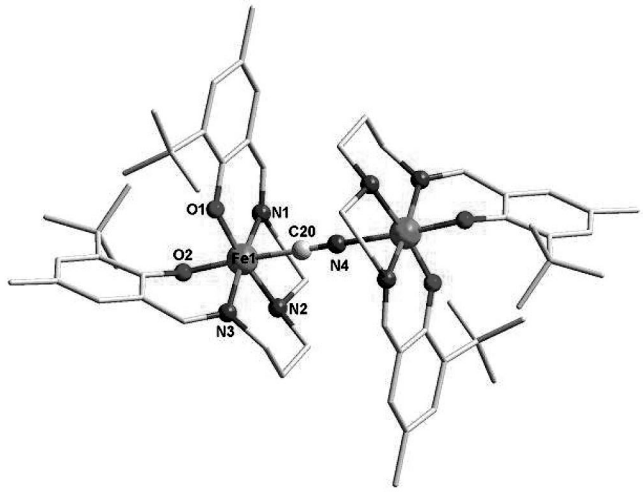

Figure 5. Molecular structure of the dinuclear complex [(MeBu-salpet)Fe{CN}$_d$Fe(MeBu-salpet)][BPh_4]·2CH_3CN [hydrogen atoms, counterions, and solvent molecules omitted for clarity; $(CN)_d$ means a disordered cyanide bridge; inversion center situated in between iron atoms]. Selected bond lengths [Å] and bridging angles [°] for **2b**: Fe1–O1 1.896, Fe1–O2 1.889, Fe1–N1 1.966, Fe1–N2 2.075, Fe1–N3 1.991, Fe1–C20 1.867, Fe1–N4 2.177; O2–Fe1–C20 176.80, O2–Fe1–N4 176.80, Fe1–C20–N4 179.08, Fe1–N4–C20 178.20.

Table 1. Overview of important bond lengths.[a]

Low-spin center			High-spin center		
Bond	Length [Å]	Average	Bond	Length [Å]	Average
[Fe(salpet)CN], L {S = 1/2} (**1c**)			[Fe(salpet)Cl], H {S = 5/2} (**1a**)		
Fe–O	1.873, 1.887	1.880	Fe–O	1.916, 1.971	1.944
Fe–N	1.904, 1.940, *2.000*	1.948	Fe–N	2.100, 2.120, *2.221*	2.147
			[Fe(MeBu-salpet)Cl], H {S = 5/2} (**1b**)		
			Fe–O	1.969, 1.897	1.933
			Fe–N	2.093, 2.093, *2.198*	2.128
			[Fe(saldpt)Cl], SIMPFE[6a]		
			Fe–O	1.935, 1.975	1.955
			Fe–N	2.113, 2.102, *2.252*	2.156
			[Fe(saldptm)Cl], XOFDOL[6b]		
			Fe–O	1.963, 1.936	1.949
			Fe–N	2.099, 2.100, *2.314*	2.171
[L^5Fe{CN}FeL^5]ClO_4·2H_2O, L^5 = salpet, LH {1/2,5/2} (**2a**)					
Fe1–O	1.915, 1.877	1.896	Fe2–O	1.938, 1.902	1.920
Fe1–N	1.929, 1.983, *2.032*	1.981	Fe2–N	2.047, 2.044, *2.139*, 2.133(NC)	2.091
[L^5Fe{CN}$_d$FeL^5][BPh_4]·2CH_3CN, L^5 = MeBu-salpet, T = 90 K (**2b**)					
Fe–O	1.896, 1.889	1.893			
Fe–N	1.966, 1.991, *2.076*	2.011[b]			
Fe–C	1.867 (disordered)				
Fe–N	2.177 (disordered)				
[L^5Fe{Fe(CN)$_5$NO}FeL^5]·0.5CH_3OH·3.75H_2O, L^5 = salpet, HH {5/2,5/2} (**3a**)					
			Fe1–O	1.951, 1.937	1.944
			Fe1–N	2.118, 2.101, *2.199*, 2.151(NC)	2.142
			Fe3–O	1.951, 1.932	1.942
			Fe3–N	2.122, 2.117, *2.209*, 2.193(NC)	2.160
[L^5Fe{Ni(CN)$_4$}FeL^5]·2CH_3OH, L^5 = MeBu-salpet, HH{5/2,5/2} (**3b**)					
			Fe–O	1.901, 1.916	1.909
			Fe–N	2.082, 2.098, *2.239*, 2.158(NC)	2.144

[a] The longest Fe–N distance corresponding to the tertiary amine is given in *italics*. [b] Bond lengths of disordered atoms are not involved in the calculation.

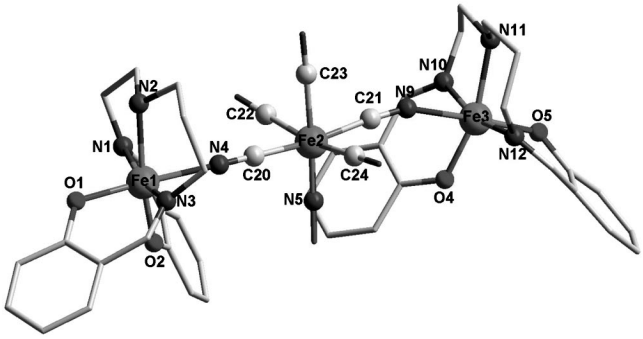

Figure 6. Molecular structure of the trinuclear complex $[\{Fe^{II}(CN)_5(NO)\}\{Fe^{III}(salpet)\}_2]\cdot 0.5CH_3OH\ 3.75H_2O$ (hydrogen atoms omitted for clarity, oxygen atoms belonging to the crystal water are fractionally occupied). Selected bond lengths [Å] for **3a**: Fe1–N1 2.118, Fe1–N2 2.199, Fe1–N3 2.101, Fe1–O1 1.955, Fe1–O2 1.951, Fe1–N4 2.151, N4–C20 1.142, Fe2–C20 1.922, Fe2–C22 1.970, Fe2–C23 1.975, Fe2–C24 1.975, Fe2–N5 1.688, Fe2–C21 1.945, C21–N9 1.137, Fe3–N9 2.193, Fe3–N10 2.117, Fe3–N11 2.209, Fe3–N12 2.122, Fe3–O4 1.932, Fe3–O5 1.951, Fe1–Fe2 5.129, Fe2–Fe3 5.158.

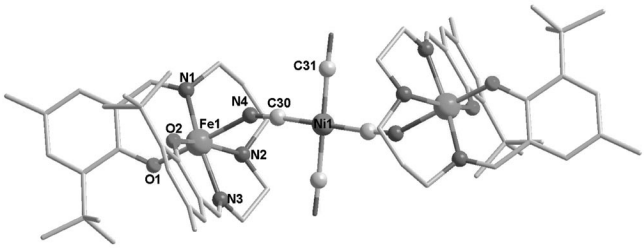

Figure 7. Molecular structure of the trinuclear complex $[\{Ni^{II}(CN)_4\}\{Fe^{III}(salpet)\}_2]\cdot 2CH_3OH$ (hydrogen atoms omitted for clarity). Selected bond lengths [Å] and bond angles [°] for **3b**: Fe1–O1 1.916, Fe1–O2 1.901, Fe1–N1 2.098, Fe1–N2 2.239, Fe1–N3 2.082, Fe1–N4 2.158; O1–Fe1–N4 178.44, Fe1–N4–C30 151.12, N4–C30–Ni1 175.70.

The above structural data are comprehensively presented in Table 1, which compares the metal–ligand distances for the low-spin and high-spin complexes under study. Notice that the bond length referring to the tertiary amine is always the longest of the Fe–N bonds.

Electronic Spectra

The electronic spectra (Figure 8) refer to the charge-transfer bands in the UV/Vis region; the spin-forbidden d–d bands ($^6A_{1g} \rightarrow {}^4T_{1g}$) are not intense enough to be recognized.

Mononuclear chlorido complex **1a** shows the first absorption band at 18000 cm^{-1} and its color is red-violet. Cyanido analogue **1c** absorbs at 13900 cm^{-1} and it is green-blue. In the UV part of the spectrum both complexes absorb at ca. 24000, 27500, and 40000 cm^{-1}.

Dinuclear complex **2a** shows the first absorption maximum at 17800 cm^{-1} with a well-visible arm at 13300 cm^{-1}; its color is in between the precursors of which it was formed: violet-blue. In the UV part of the spectrum it shows absorptions characteristic for its precursors.

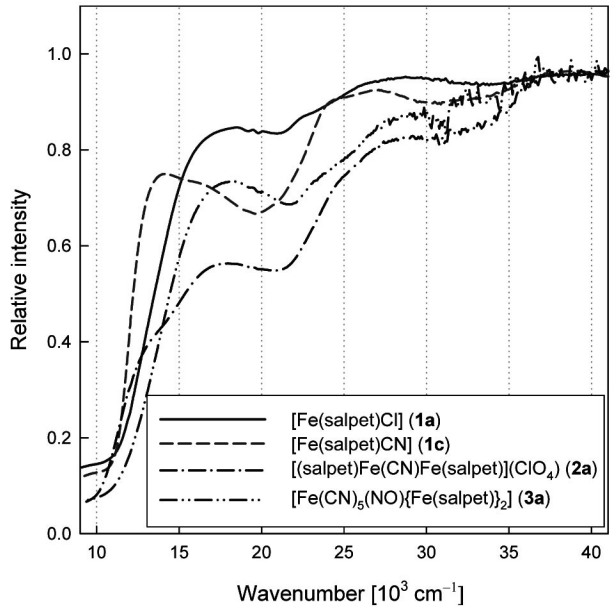

Figure 8. Solid-state electronic spectra of salpet-containing complexes **1a**, **1c**, **2a**, and **3a** at room temperature.

The absorptions of trinuclear complex **3a** are analogous to mononuclear weak-field complex **1a**.

Magnetic Data for Single-Reference Systems

The magnetic data for two mononuclear complexes (**1a** and **1c**) and one trinuclear complex (**3b**) can be fitted with a traditional, single-reference spin Hamiltonian. However, in contrast to the usual approach, the susceptibility data set and the magnetization data set were treated simultaneously so that the retrieved magnetic parameters should reproduce both magnetic functions.

The mononuclear complex $[\{Fe^{III}(salpet)(Cl)\}]$ (**1a**) is high spin, $S = 5/2$. Its effective magnetic moment at room temperature is $\mu_{eff} = 5.7\,\mu_B$ and it slowly decreases upon cooling (Figure 9). This reflects the Curie law fulfilled at higher temperature with some temperature-independent paramagnetism (TIP). On cooling below 25 K the value of μ_{eff} drops to $\mu_{eff} = 3.3$ at $T = 1.8$ K. The molecular-field correction is not the raison d'etre of the lowered magnetic productivity, as it cannot reproduce the suppressed low-temperature magnetization at 5 T. The fitting procedure gave $g_H = 1.813$, $D/hc = 1.52\ cm^{-1}$, $E/hc = 0.33\ cm^{-1}$, and $\chi_{TIP} = 4.99 \times 10^{-9}\ m^3\,mol^{-1}$ [discrepancy factor $R(\chi) = 0.010$]. The reduction in the g-factor with respect to the spin-only value may originate in the very distorted chromophore of the complex.

The high-spin state of **1a** was also confirmed by Mössbauer spectra: the quadrupole splitting ($Q = 0.7$) and the isomer shift ($\delta = 0.3$) change only a little when the temperature was increased from $T = 20$ K to room temperature (all MS data in units of $mm\,s^{-1}$).

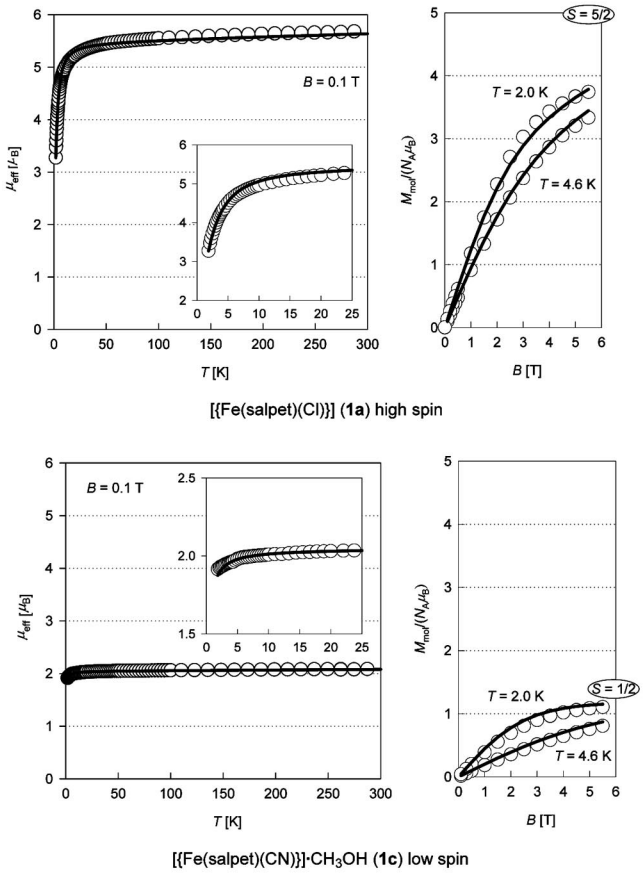

Figure 9. Magnetic data for mononuclear Fe^{III} complexes **1a** and **1c**. Temperature dependence of the effective magnetic moment (left); field dependence of the magnetization (right). Solid lines represent fitted data.

Mononuclear complex [{Fe^{III}(salpet)(CN)}]·CH_3OH (**1c**) is low spin owing to the high crystal-field strength of the cyanido ligand (Figure 9). For $S = 1/2$ paramagnet the Curie law provides a straight-line temperature development of μ_{eff}; this should be improved by TIP, as well as by the molecular field corrections (operative at low temperature). The magnetic parameters $g_L = 2.36$, $\chi_{TIP} = 0.76 \times 10^{-9}$ $m^3 mol^{-1}$, and $zj/hc = -0.17$ cm^{-1} reproduce the susceptibility satisfactorily [$R(\chi) = 0.019$]. The *g*-value shows some orbital contribution within the {FeN_3O_2C} chromophore relative to the spin-only value. In a hypothetical octahedral geometry the reference crystal-field term $^2T_{2g}$ is orbitally degenerate and the Griffith/Figgis model of symmetry lowering would be more appropriate than the spin Hamiltonian formalism.[5]

The magnetic functions for complex **3b** show features typical for the HH pair of Fe^{III} centers coupled in a ferromagnetic manner (Figure 10). The very central, square-planar $\{Ni^{II}(CN)_4\}^{2-}$ unit is diamagnetic. Upon cooling, the effective magnetic moment stays approximately constant and below 30 K it starts to increase. The magnetization saturates to a value of $M_1 = M_{mol}/N_A\mu_B = 10$ [T = 2.0 K, B = 5.5 T]. In our classification this system refers to the class A/HH. The magnetic data could be fitted with the isotropic exchange model (J and g_H) but some zero-field splitting parameter (D_H) leads to a better reproduction of the low-temperature data sets: $g_H = 2.010$, $J/hc = +0.085$ cm^{-1}, $D_H/hc = 0.45$ cm^{-1} [$R(\chi) = 0.019$, $R(M) = 0.013$].

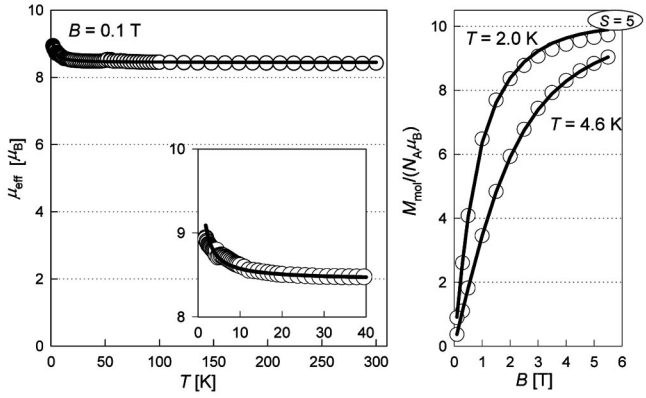

Figure 10. Magnetic data for the trinuclear complex [$L^5Fe^{III}\{Ni^{II}(CN)_4\}Fe^{III}L^5$]·$2CH_3OH$ (**3b**). Temperature dependence of the effective magnetic moment (left); field dependence of the magnetization (right). Open circles represent the experimental data, whereas solid lines represent the fitted data.

Mössbauer Spectra

Dinuclear complex **2a** possesses inequivalent Fe^{III} centers. The *C*-coordinated center is expected to be low spin, whereas the *N*-coordinated one is to be high spin. Such a single LH reference state would exhibit 50% of the high-spin mole fraction in the MS spectra over the whole temperature region. The recorded spectra, however, show a more complex situation (Figure 11). Their characteristics for the low-spin centers ($Q = 2.56$, 2.36; $\delta = 0.047$, –0.028) and the high-spin centers ($Q = 0.96$, 0.90; $\delta = 0.308$, 0.293) change little between $T = 20$ and 300 K, respectively. However, the corresponding area fraction (A) rises in favor of the high-spin state (from 38 to 61% of the HS fraction). This excludes constant amounts 50% of LS and 50% of HS and unambiguously shows that the dinuclear complex exhibits a kind of spin crossover. The lower value of $x_{HS} = 0.38$ at $T = 20$ K arises from thermal population of the LL state that lies close to the LH one. On the contrary, the increased value of $x_{HS} = 0.61$ at $T = 300$ K arises from a thermal population of the HH state.

The Mössbauer spectra for trinuclear complex **3a** (Figure 12) show a coexistence of the low-spin and high-spin Fe^{III} centers even at temperatures as low as $T = 20$ K. The spectra are complex, because the Fe^{III} centers are not perfectly equivalent. Deconvolution to three quadrupole doublets shows that upon warming a spin crossover proceeds: the Fe^{III} center passes from the low-spin state to the high-spin one.

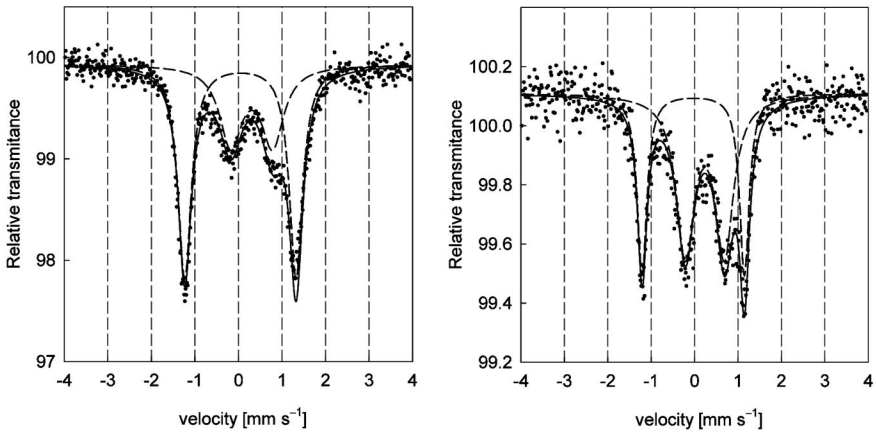

Figure 11. Mössbauer spectra of dinuclear complex **2a**. Dashed lines represent deconvolution to the LS and HS quadrupole doublets. Left: T = 20 K, Q1 2.56, δ1 0.047, A1 62%, Q2 0.96, δ2 0.308, A2 38% (R = 0.102%); right: T = 300 K, Q1 2.36, δ1 –0.028, A1 39%, Q2 0.90, δ2 0.239, A2 61% (R = 0.053%).

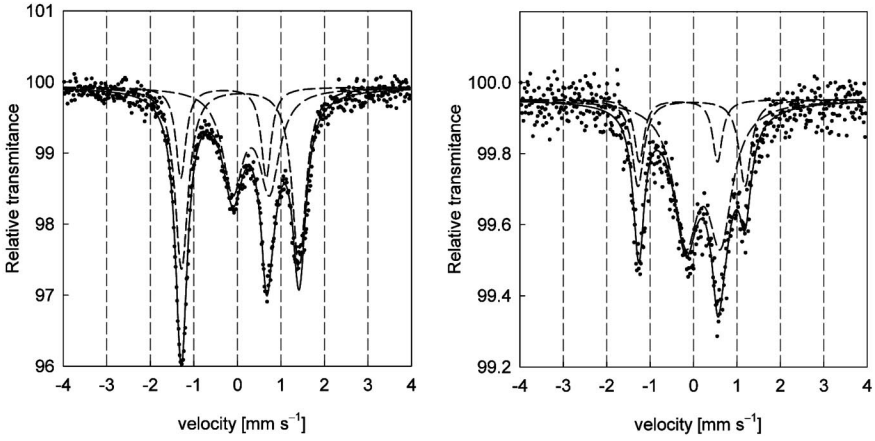

Figure 12. Mössbauer spectra of trinuclear complex **3a**. Dashed lines represent deconvolution to three quadrupole doublets. Left: T = 20 K: Q1 2.70, δ1 0.073, A1 46%, Q2 0.85, δ2 0.323, A2 38%, Q3 1.95, δ3 –0.319, A3 16% (R = 0.126%). Right: T = 300 K: Q1 2.46, δ1 –0.044, A1 22%, Q2 0.80, δ2 0.222, A2 65%, Q3 1.80, δ3 –0.346, A3 13% (R = 0.043%).

Theoretical Model for Multicenter Spin Crossover

The existing spin crossover models proposed for the dinuclear systems are heavily oversimplified because of the following drawbacks.[3b,7] (1) They assume that the HL and LH pairs are equivalent (which is not the case for cyanido-bridged complexes) and that they lie in between the LL and HH reference states. (2) Moreover, they were developed to fit the high-spin mole fraction and not the primary experimental data (susceptibility and magnetization). (3) They ignore the role of the exchange interaction by assuming that this is irrelevant. (4) They do not include the vibrational partition function for dinuclear complexes. It is not surprising that their application to the present data on cyanido-bridged complexes was unsuccessful. Therefore we outlined a more general and more flexible model that could be applied in a direct fitting of magnetic data (temperature dependence of the magnetic susceptibility, field dependence of the magnetization). Its essential features follow. (1) Each of four reference states, that is, AB = LL, LH, HL, and HH, can be characterized by a common spin Hamiltonian that involves the isotropic exchange coupling and the spin Zeeman term [Equation (1)].

$$\hat{H}_{AB}^{\text{spin}} = -J_{AB}(\vec{S}_A \cdot \vec{S}_B)\hbar^{-2} + \mu_B B(g_A\vec{S}_A + g_B\vec{S}_B)\hbar^{-1} \quad (1)$$

When necessary, the Hamiltonian can involve the asymmetric exchange appropriate to the LL state (D_{LL} parameter) and the single-ion zero-field splitting term appropriate to the LH and HH states (D_{H} parameter). (2) For the LL pair there are 4 energy levels $\varepsilon_{\text{LL}}(S, M_S)$ with $S \in <0, 1>$, for the LH (HL) pair there are 12 energy levels $\varepsilon_{\text{LH}}(S, M_S)$ with $S \in <2, 3>$, and for the HH pair there are 36 energy levels $\varepsilon_{\text{HH}}(S, M_S)$ with $S \in <0, 5>$. The construction of matrix elements in the basis set of either coupled or uncoupled spin-kets is a matter of routine. For the field dependence, three magnetic fields are selected near the reference, say $B_{r,k} = B_r$, $B_r + \delta$, and $B_r + 2\delta$, where δ is a small field increment. The eigenvalue routine returns three sets of energy levels for

the given field direction $\varepsilon_{AB,i}(B_{r,k})$. (3) The total partition function of the system is constructed according to Equation (2).

$$Z(B_{r,k},T) = z_{\mathrm{LL}} \cdot \sum_{i=1}^{4} \exp[-(\Delta_{\mathrm{LL}} + \varepsilon_{\mathrm{LL},i,r,k})/kT] + z_{\mathrm{LH}} \cdot \sum_{i=1}^{12} \exp[-(\Delta_{\mathrm{LH}} + \varepsilon_{\mathrm{LH},i,r,k})/kT] + z_{\mathrm{HL}} \cdot \sum_{i=1}^{12} \exp[-(\Delta_{\mathrm{HL}} + \varepsilon_{\mathrm{HL},i,r,k})/kT] + z_{\mathrm{HH}} \cdot \sum_{i=1}^{36} \exp[-(\Delta_{\mathrm{HH}} + \varepsilon_{\mathrm{HH},i,r,k})/kT] \quad (2)$$

Here, the energy separations, $\Delta_{\mathrm{LL}} = 0$, Δ_{LH}, Δ_{HL}, and Δ_{HH}, need be considered as external parameters, as they do not enter the spin Hamiltonian. They originate in the orbital angular momentum and relate to the actual crystal-field strength in the complex under study. Normally, $\Delta_{\mathrm{LH}} = \Delta_{\mathrm{HL}}$ is assumed for symmetric centers; however, this is not generally fulfilled. It is assumed that the vibrations of individual centers are independent and thus the vibration partition function for a pair of centers is a product $z_{AB} = z_A z_B$. To a further approximation the averaged vibration frequencies $\bar{\nu}_{\mathrm{H}}$ and $\bar{\nu}_{\mathrm{L}}$ were introduced (Einstein modes); hence, the term given by Equation (3).

$$z_A = \frac{\exp[-(mh\bar{\nu}_A/2)/kT]}{[1-\exp(-h\bar{\nu}_A/kT)]^m} \quad (3)$$

For a hexacoordinate metal center the number of active modes amounts to $m = 15$. (4) The molar magnetization is defined through the first derivative of the partition function at the reference field B_r [Equation (4)].

$$M_{\mathrm{mol}}(B_r,T) = N_{\mathrm{A}}kT\left(\frac{\partial \ln Z}{\partial B}\right)_{B_r} = N_{\mathrm{A}}kT(c_T^{(1)} + 2c_T^{(2)}B_r) \quad (4)$$

The logarithm of the partition function was fitted by a parabola term [Equation (5)].

$$\ln Z(B_r,T) = c_T^{(0)} + c_T^{(1)}B_r + c_T^{(2)}B_r^2 \quad (5)$$

(5) At a low magnetic field ($B_0 = 0.1$ T) we are left with a linear magnetic material and thus the magnetic susceptibility results in Equation (6).

$$\chi_{\mathrm{mol}}(B_0,T) = \mu_0\left(\frac{\partial M_{\mathrm{mol}}(B)}{\partial B}\right)_{B_0} = \mu_0 N_{\mathrm{A}}kT(2c_T^{(2)}) \quad (6)$$

(6) The high-spin mole fraction is calculated by the term given in Equation (7).

$$x_{\mathrm{HS}} = (0\cdot P_{\mathrm{LL}} + 1\cdot P_{\mathrm{LH}} + 1\cdot P_{\mathrm{HL}} + 2\cdot P_{\mathrm{HH}})/2 \quad (7)$$

This quantity is comparable to the area fraction detected in Mössbauer spectra. Here the Boltzmann population factors are given by Equation (8).

$$P_{AB} = \{z_{AB} \cdot \sum_{i=1} \exp[-(\Delta_{AB} + \varepsilon_{AB,i})/kT]\}/Z \quad (8)$$

The outlined procedure could work properly on assuming that there is not a substantial solid-state cooperativeness (an extra interaction energy preferring the spin-like pairs). The solid-state cooperativeness could be accounted by modifying the spin-crossover model for dinuclear systems as proposed by Bousseksou.[7] In the present case the solid-state cooperativeness is neglected.

The minimum parameter set covers g_{L}, g_{H} (≈ 2), J_{LL}, J_{LH} ($= J_{\mathrm{HL}}$), J_{HH}, D_{H}, D_{LL}, $\Delta_{\mathrm{LH}} = \Delta_{\mathrm{HL}}$, Δ_{HH}, and $h\bar{\nu}_{\mathrm{L}} = 1.15(h\bar{\nu}_{\mathrm{H}})$. One can argue that the parameter set is too extensive and the model overparametrized. The experience shows that simplified versions do not work properly. A single data set (say the temperature dependence of the susceptibility) is surely incapable to fix such a numerous set of parameters reliably. Different experimental functions are sensitive to different parameters. For instance, the magnetization data set determines the g and D parameters. Therefore, by treating three different data sets simultaneously {$\chi = f_1(T)$, $M = f_2(B,[T])$ and $x_{\mathrm{HS}}^{(\mathrm{MS})} = f_3(T)$} we arrived at the minimum of the postulated functional term [Equation (9)]

$$F(\ldots p_i \ldots) = w_1(1/n)\sum_n^N \left|\frac{\chi_n^{\mathrm{o}} - \chi_n^{\mathrm{c}}}{\chi_n^{\mathrm{o}}}\right| + w_2(1/m)\sum_m^M \left|\frac{M_m^{\mathrm{o}} - M_m^{\mathrm{c}}}{M_m^{\mathrm{o}}}\right| + w_3(1/k)\sum_k^K \left|\frac{x_k^{\mathrm{o}} - x_k^{\mathrm{c}}}{x_k^{\mathrm{o}}}\right| \quad (9)$$

by using advanced methods of nonlinear optimization (a simulated annealing method and genetic algorithm). Several dozens of initial trials and several thousands of optimization steps were tested to identify the stationary solution.

Magnetic Data for Spin Crossover Systems

Complex **2a** shows a gradual increase in its effective magnetic moment with temperature between $\mu_{\mathrm{eff}} = 5.04\ \mu_{\mathrm{B}}$ at $T = 4.2$ K and $\mu_{\mathrm{eff}} = 6.08\ \mu_{\mathrm{B}}$ at $T = 300$ K (Figure 13). The magnetization per formula unit approaches a value of $M_1 = 3.5$ [$T = 2.0$ K, $B = 5.5$ T]. This refers neither to the pure ground LL state [$M_{(S=1)} = 2$] nor the LH state [$M_{(S=3)} = 6$]. Thus, we are left with the conclusion that the separation of these states, Δ_{LH}, need be small and both states are populated at temperatures as low as $T = 2.0$ K. The HH state lies at a much higher energy, which causes a weak increase in the effective magnetic moment above 150 K.

The results of the fitting procedure are compiled in Table 2. The calculated values of $\Delta_{\mathrm{LH}}/k = 4.51$ K and $\Delta_{\mathrm{HH}}/k = 903$ K match the above expectations. These values confirm a classification of the ground state as class-B/LL+LH. Notice that the energy of the HL pair was artificially lifted outside the thermal population, $\Delta_{\mathrm{HL}}/k > 10000$ K, in order to exclude an improbable situation that the C-coordinated Fe^{III} center is high spin and the N-coordinated Fe^{III} center is low spin. The calculated value of the mean vibrational

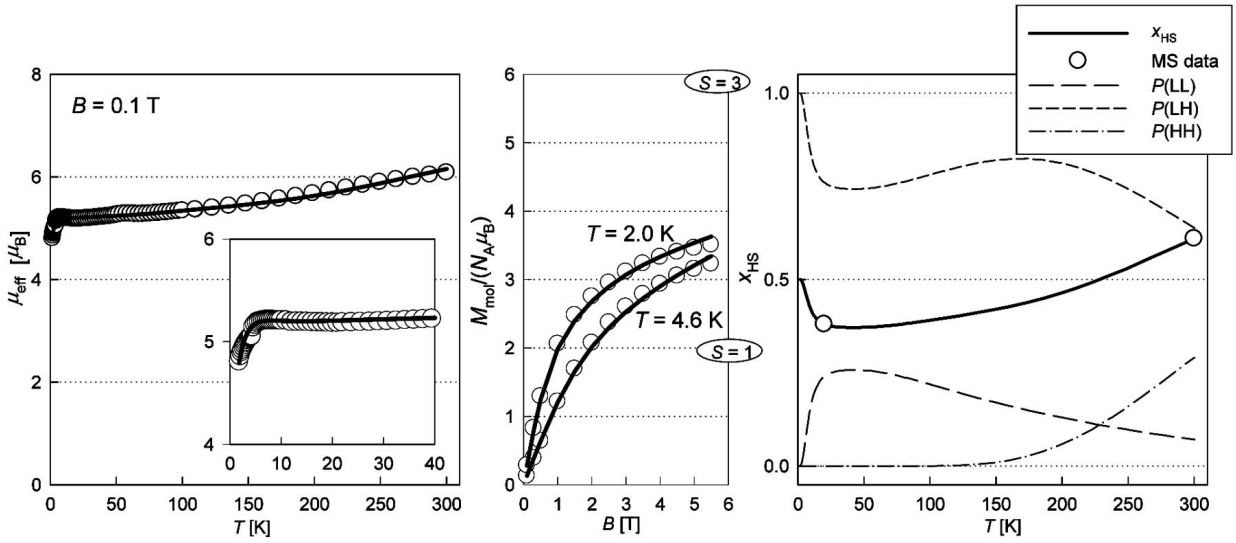

Figure 13. Magnetic data for the dinuclear complex [(salpet)Fe{CN}Fe(salpet)]ClO_4·2H_2O (**2a**). Temperature dependence of the effective magnetic moment (left); field dependence of the magnetization (middle); high-spin mole fraction and Boltzmann population factors (right). Open circles represent experimental data, whereas solid lines represent fitted data.

frequency refers to the wavenumber $\bar{\nu}_H$ = 238 cm^{-1} ($\bar{\nu}_L/\bar{\nu}_H$ = 1.16), which spans the experimental range known for mononuclear Fe^{III} complexes. For instance, six skeletal vibrational modes for the {$Fe^{III}N_4O_2$} chromophore in the high-spin state were detected between 182 and 531 cm^{-1}.[8]

Table 2. Calculated spin Hamiltonian and spin-crossover parameters.

Parameter	**2a**	**2b**, set-a, LL+LH	**2b**, set-b, LH	**3a**
g_L	2.65	2.90	3.00	2.89
g_H	1.80	1.80	1.81	2.00
(J_{LL}/hc) [cm^{-1}]	–3.93	–3.93	–	–7.62
(J_{LH}/hc) [cm^{-1}]	–0.16	–31.0	–27.0	–0.33
(J_{HH}/hc) [cm^{-1}]	–3.67	–6.31	–7.59	–0.68
(D_{LL}/hc) [cm^{-1}]	–1.77	–19.3	–	–7.39
(D_H/hc) [cm^{-1}]	–4.20	–27.0	–23.9	–2.68
(Δ_{LH}/k) [K]	4.51[a]	9.72[a]	0[b]	1.70[c]
(Δ_{HH}/k) [K]	903	300	431	550
$\bar{\nu}_H$ [cm^{-1}]	238	100	151	116
$\bar{\nu}_L/\bar{\nu}_H$	1.16	1.13	1.17	1.10
$R(\chi)$[d]	0.020	0.016	0.017	0.042
$R(M)$	0.022	0.059	0.047	0.052
$R(x_{HS})$	0.0006	–	–	0.11

[a] Fixed value Δ_{HL}/k = 10000 K. [b] Δ_{LL}/k = 10000 K. [c] Δ_{HL} = Δ_{LH}. [d] $R(p)$ = discrepancy factors for property p.

The reader could be a bit frustrated why the calculated g_H-factors for the {Fe–CN–Fe} moieties adopt "subnormal" values. No doubts that the –CN ligand brings not only a strong crystal field but also a considerable covalence (modeled by the orbital reduction factors). These factors are associated with the orbital angular momentum and thus they are not recovered by the spin Hamiltonian. In reality, four different g-factors come into consideration: $g_L(Fe_1–C)$, $g_H(Fe_1–C)$, $g_L(Fe_2–N)$, and $g_H(Fe_2–N)$; their fixing is not a reliable task and, moreover, they can be anisotropic. Therefore the above-reported isotropic g_H or g_L values need be considered as effective, model-dependent parameters that mimic an overall evolution of the Zeeman levels in an applied magnetic field.

The reconstructed energy levels and the individual Boltzmann population factors are plotted in Figure 13 along with the high-spin mole fraction x(HS). The last quantity matches perfectly with that subtracted from the Mössbauer spectra data.

Also, dinuclear complex **2b** exhibits a kind of spin crossover (Figure 14). On heating above 4 K, the effective magnetic moment stays constant, μ_{eff} = 3.2 μ_B until T = 30 K; this value matches the presence of the LL pair. The magnetization, surprisingly, saturates to a subnormal value of M_1 = 1.27 [T = 2.0 K, B = 7 T], which is much lower than $M_{(S=1)}$ = 2 expected for the LL pair. This feature indicates a presence of very strong single-ion anisotropy (D_H), or the asymmetric exchange (D_{LL}, D_{LH}).

Using vector-coupling algebra, the D values for the given spin arise in the form: (i) for the LL pair $D_{(S=1)}$ = (1/2)D_{LL}; (ii) for the LH pair $D_{(S=2)}$ = (4/3)D_H – (1/6)D_{LH}, and $D_{(S=3)}$ = (2/3)D_H + (1/6)D_{LH}; the triplet is split into levels lying at 0, D (M_S = ±1); the quintet to 0, D (M_S = ±1), 4D (M_S = ±2) sublevels; the septet to the 0, D (M_S = ±1), 4D (M_S = ±2), and 9D (M_S = ±3) manifolds.[9] Because D_H, D_{LL}, and D_{LH} can adopt either negative or positive values, we are left with a serious problem of fixing them. A rather abrupt increase in the magnetization for **2b** is a fingerprint of D_S < 0 for the ground state, which gives an assumption for D_H to be large and negative. In a similar manner, the g-factors are coupled as follows: (i) for the LL pair $g_{(S=1)}$ = (1/2)g_{L1} + (1/2)g_{L2}; for the LH pair $g_{(S=2)}$ = (–1/6)g_{L1} + (7/6)g_{H2}, and $g_{(S=3)}$ = (1/6)g_{L1} + (5/6)g_{H2}.

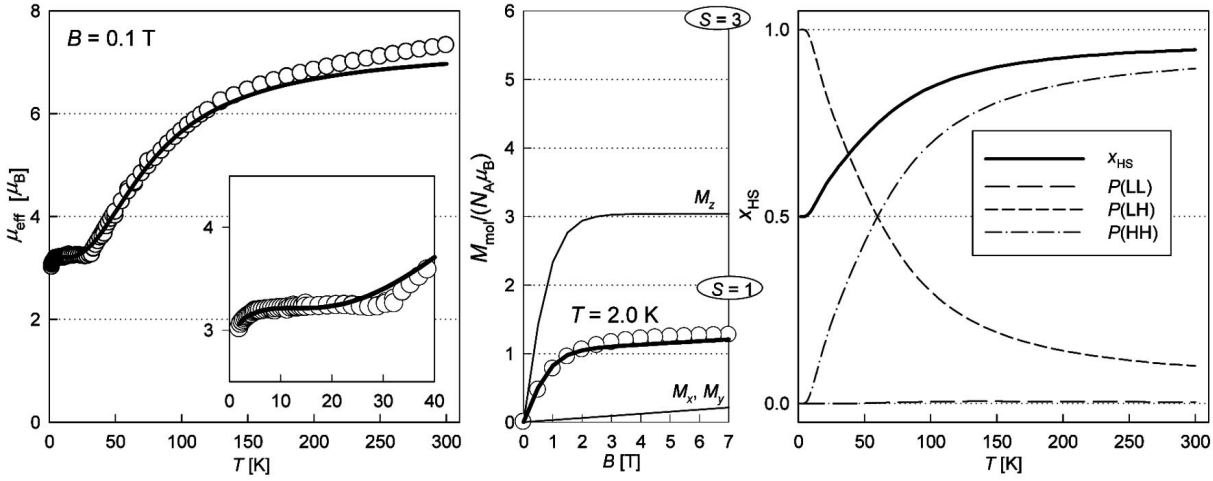

Figure 14. Magnetic data for the dinuclear complex [(MeBu-salpet)Fe{CN}$_d$Fe(MeBu-salpet)][BPh_4]·2CH_3CN (**2b**). Temperature dependence of the effective magnetic moment (left); field dependence of the magnetization (middle); high-spin mole fraction and Boltzmann population factors (right). Open circles represent experimental data, whereas solid lines represent fitted data.

Assuming that the ground state of **2b** arises from the LH pair coupled in an antiferromagnetic manner, with $D < 0$ the $M_S = \pm 3$ pair will be well separated from the rest of the energy spectrum. The Zeeman energy levels are $\varepsilon^z_{1,2} = \pm 3 g_z \mu_B B$ and $\varepsilon^x_{1,2} = +(3/10D)(g_x \mu_B B)^2$ (at a small field, $D >> g_x \mu_B B$), and the magnetization components per particle become Equations (10) and (11).

$$M_z/(N_A\mu_B) = 3g_S[\exp(+3g_S\mu_B B/kT) - \exp(-3g_{S\mu_B}B/kT)] / [\exp(+3g_S\mu_B B/kT) + \exp(-3g_S\mu_B B/kT)] \quad (10)$$

$$M_x/(N_A\mu_B) = -(3/10D)2g_S^2\mu_B B \quad (11)$$

The modeling brings a result that the in-plane component M_x (M_y) raises only slightly in moderate fields and consequently the averaged magnetization is much lower with respect to the Brillouin function behavior. Moreover, if only the LH pair is populated (and not HL) then the overall contribution to the molar magnetization is a half of the formula unit (Figure 14). A hand calculation brings an estimate $M_{av}/(N_A\mu_B) = (1/2)(2M_x + M_z)/3 = 0.5 \cdot (2.0 + 6)/3 = 1$, which matches the observation.

The fitting procedure for **2b** was conducted in two ways. Set "a" closely resembles the procedure applied for **2a** (Table 2). Indeed, the ($J + D$) splitting causes the ground state to refer to the $M_S = \pm 3$ doublet arising from the $S = 3$ multiplet of the LH reference. After the first energy gap, the remaining energy levels form a broad band; its Boltzmann population results in a gradual spin crossover. It seems that the presence of the LL reference is ineffective and therefore this state has been lifted out of the thermal population (set "b"). To this end, almost the same quality of the fit and almost the same set of parameters were retrieved (Figure 15).

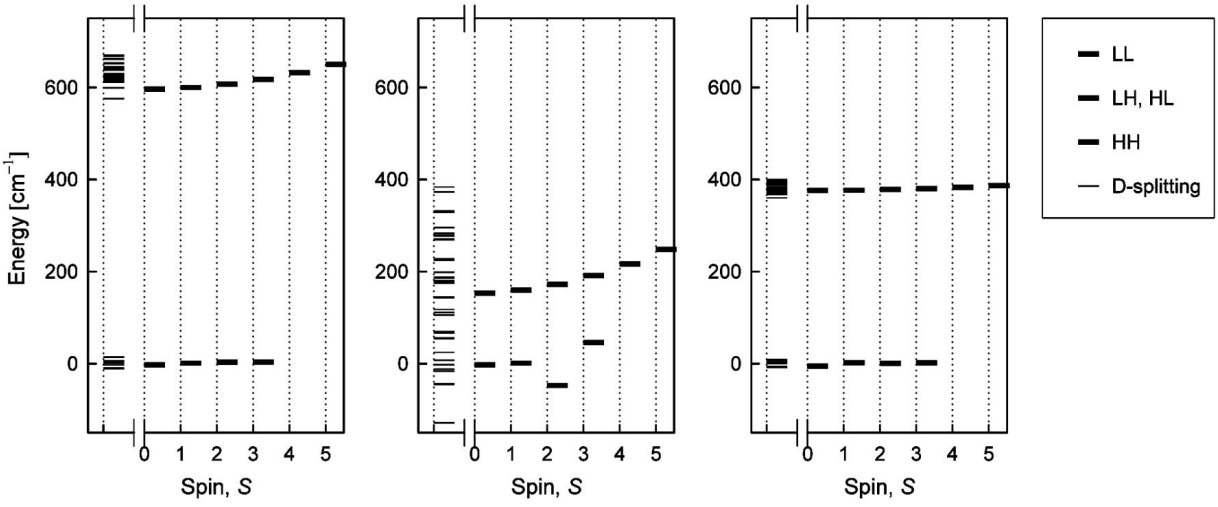

Figure 15. Calculated energy levels for **2a**, **2b**, and **3a**. First column – whole spectrum resulting from the asymmetric exchange; levels attached to a definite S – within the isotropic exchange.

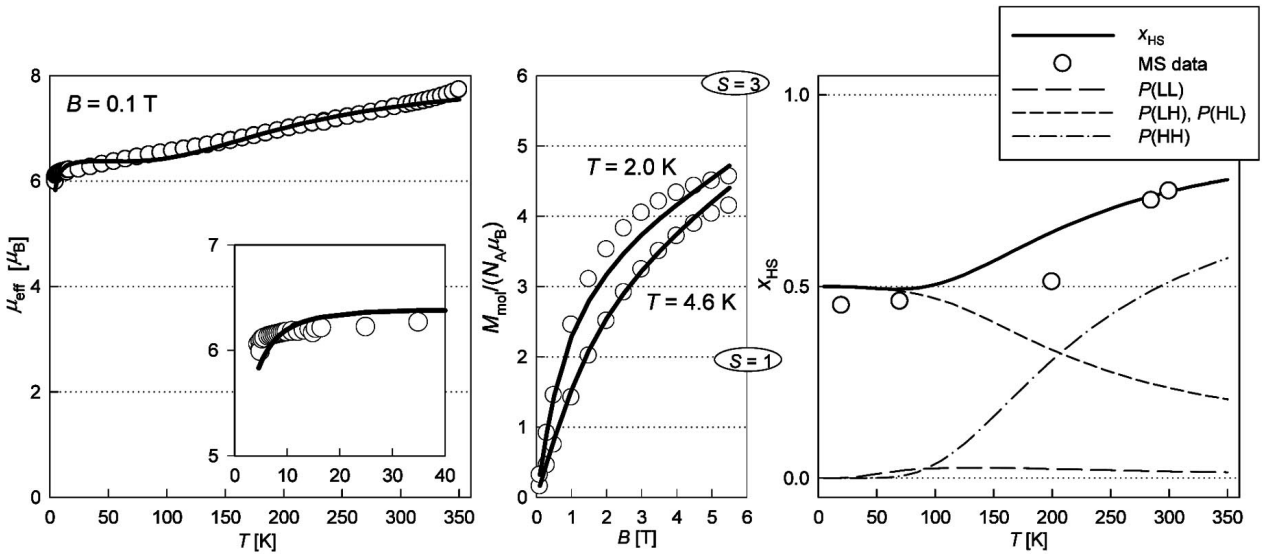

Figure 16. Magnetic data for trinuclear complex **3a**. Temperature dependence of the effective magnetic moment (left); field dependence of the magnetization (middle); high-spin mole fraction and Boltzmann population factors (right). Open circles represent experimental data, whereas solid lines represent fitted data.

Complex **3a** consists of a diamagnetic central unit $\{Fe^{II}(CN)_5(NO)\}$ and therefore it behaves magnetically like a dinuclear Fe^{III} complex. The magnetic data measured until T = 350 K reveal that at the highest temperature $\mu_{eff} \approx 7.7\ \mu_B$, whereas at T = 4 K, $\mu_{eff} \approx 6.0\ \mu_B$ holds true (Figure 16). The magnetization of $M_1 = 4.5\ \mu_B$ [T = 2.0 K, B = 5.5 T] indicate that in addition to the LL state the LH (=HL) state is also populated. Thus, $E_{LL} \approx E_{LH} = E_{LH} << E_{HH}$ need be fulfilled for the reference states. The magnetic data (Table 2) are in a harmony with the Mössbauer spectra showing that a type of spin crossover proceeds: at T = 20 K the renormalized area fraction is 0.45 for Fe^{III}–HS; at T = 300 K this is 0.75.

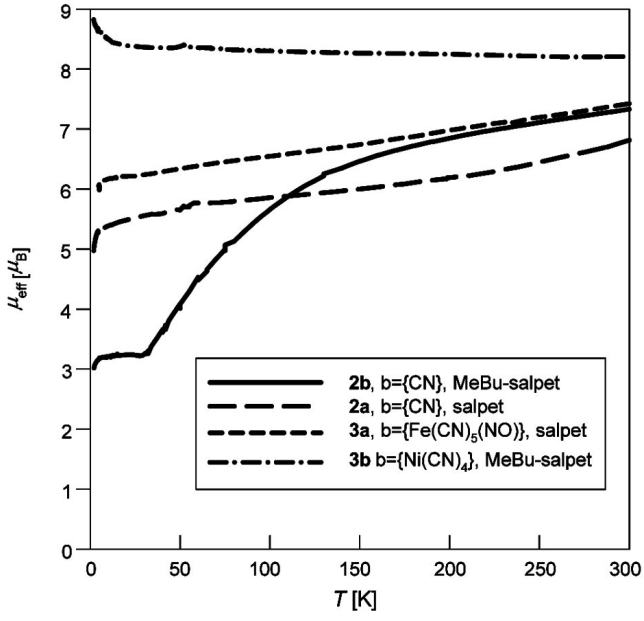

Figure 17. Comparison of magnetic data for spin crossover and high-spin dinuclear and trinuclear complexes linked by a diamagnetic bridge b.

Conclusions

A traditional view to the spin crossover in dinuclear complexes assumes that upon heating the low-spin pair (LL) is transformed into the high-spin pair (HH). Relatively little is known about the role of the LH (and HL) pairs, assumed to be present in between the LL and HH ones.

We prepared and structurally characterized two dinuclear CN-bridged complexes, **2a** and **2b**, and a mixed-valence trinuclear complex, **3a**, where the role of the LH pair is essential for spin crossover (Figure 17). The LH reference state can be well isolated, or interacting with the LL one through an overlap of their energy subbands made by the exchange interaction. It can be concluded that the spin crossover interferes with the exchange interactions in this class of complexes.

Experimental Section

Ligands: The Schiff-condensation of (substituted) *o*-salicylaldehyde with an aliphatic amine 1,6-diamino-4-azahexane (abbr. *pet*) $H_2N(CH_2)_3NH(CH_2)_2NH_2$ at a ratio of 2:1 resulted in pentadentate ligands (yellow oils) according to Figure 18.

Mononuclear Complex [Fe(salpet)Cl] (1a): A methanol solution of H_2salpet (5 mmol in 15 mL) was combined with a methanol solution of $FeCl_3 \cdot 6H_2O$ (5 mmol in 30 mL) accompanied with color change to dark violet. Then, triethylamine (10 mmol) was added. After 30 min of stirring at 50 °C the reaction mixture was cooled to room temperature and a dark-brown crystalline powder precipitated. This was separated by filtration, washed with cold methanol and ethyl ether. Yield: 1.67 g (85%). $C_{19}H_{21}ClFeN_3O_2$ (414.69):

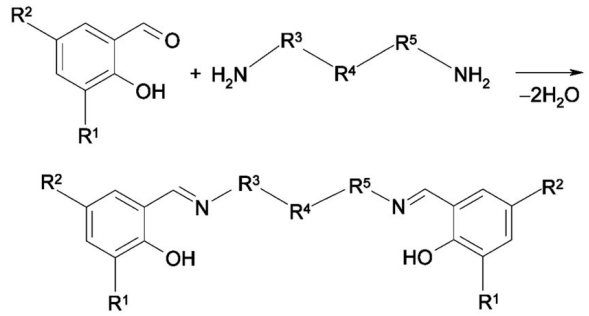

Figure 18. Schiff condensation resulting in H_2salpet ($R^1 = R^2 = H$, $R^3 = CH_2CH_2CH_2$, $R^5 = CH_2CH_2$, $R^4 = NH$) and H_2MeBu-salpet [$R^1 = tert$-$(CH_3)_3C$, $R^2 = CH_3$, $R^3 = CH_2CH_2CH_2$, $R^5 = CH_2CH_2$, $R^4 = NH$]; H_2salpet = *N*,*N*′-bis(1-hydroxy-2-benzyliden)-1,6-diamino-4-azahexane.

calcd. C 55.0, H 5.07, N 10.1, Fe 13.5; found C 54.3, H 5.10, N 10.1, Fe 12.6. IR (KBr): $\tilde{\nu}$ = 3230 (N–H); 1631, 1620, 1597 (C=N) cm^{-1}. UV/Vis (nujol): $\tilde{\nu}$ = 18000, 24000, 27500, 40000 cm^{-1}. χ_{dia} = -2.78×10^{-9} $m^3 mol^{-1}$.

Mononuclear Complex [Fe(MeBu-salpet)Cl] (1b): A methanol solution of $FeCl_3 \cdot 6H_2O$ (10 mmol in 50 mL) was added to solution of H_2MeBu-salpet (10 mmol in 30 mL of methanol mixed with 20 mL of *n*-butanol). The mixture was stirred at 50 °C for 15 min and then triethylamine (22 mmol) was added. The resulting solution was stirred at 50 °C for 10 min and after cooling a black crystalline powder precipitated. This was collected, washed with methanol and ethyl ether, and dried in vacuo. Yield: 4.94 g (89%). $C_{29}H_{41}ClFeN_3O_2$ (554.95): calcd. C 62.8, H 7.45, N 7.57; found C 61.2, H 7.60, N 7.40. IR (KBr): $\tilde{\nu}$ = 3213 (N–H); 1625, 1604 (C=N); 1270 (C–O). χ_{dia} = -4.27×10^{-9} $m^3 mol^{-1}$.

Mononuclear Complex [Fe(salpet)CN]·CH_3OH (1c): A methanol solution of [Fe(salpet)Cl] (1 mmol in 40 mL) was combined with a water solution of KCN (5% excess relative to the stoichiometric amount). After short stirring, the color turned from red to dark blue and a black crystalline powder precipitated. This was separated by filtration, washed with cold methanol and ethyl ether. Yield: 0.40 g (92%). $C_{21}H_{25}FeN_4O_3$ (437.29): calcd. C 57.8, H 5.76, N 12.8, Fe 12.8; found C 57.0, H 5.45, N 12.5, Fe 12.6. IR (KBr): $\tilde{\nu}$ = 3194 (N–H); 1630, 1615, 1601 (C=N); 2111 (C≡N); 3375 (O–H). UV/Vis (nujol): $\tilde{\nu}$ = 13900, 24000, 27500, 40000. χ_{dia} = -2.93×10^{-9} $m^3 mol^{-1}$.

The above mononuclear precursors are water-sensitive. They are soluble in methanol, ethanol, acetonitrile, chloroform, and toluene.

Dinuclear Complex [Fe(salpet){CN}Fe(salpet)](ClO_4)·$2H_2O$ (2a): An acetonitrile solution of [Fe(salpet)CN] (1 mmol in 40 mL) was combined with a methanol solution of $Ni(ClO_4)_2 \cdot 6H_2O$ (0.25 mmol in 5 mL). The mixture was stirred for 2 h at 50 °C and then left to evaporate spontaneously for several days at room temperature. Black crystals were separated by filtration. Yield: 0.33 g (72%). $C_{39}H_{46}ClFe_2N_7O_{10}$ (919.70): calcd. C 50.9, H 5.01, N 10.7; found C 50.5, H 4.69, N 10.5. IR (KBr): $\tilde{\nu}$ = 3194 (N–H); 1631, 1619, 1598 (C=N); 2132 (C≡N). UV/Vis (nujol): $\tilde{\nu}$ = 13300, 17800. χ_{dia} = -5.99×10^{-9} $m^3 mol^{-1}$.

Dinuclear Complex [Fe(MeBu-salpet){CN}Fe(MeBu-salpet)][BPh_4]·$2CH_3CN$ (2b): To a methanol/acetonitrile solution (1:1, 100 mL) of [Fe(MeBu-salpet)Cl] (1.25 mmol) and K[$Ag(CN)_2$] (1 mmol) was added and the suspension was stirred for 1.5 h. Resulting solution was filtered off to a solution of $NaBPh_4$ (0.65 mmol in 5 mL) and left to cool down. After 3 h green-brown crystals of good quality were formed and these were separated by filtration, washed by cold methanol and ethyl ether. Yield: 0.81 g (88%). $C_{87}H_{108}BFe_2N_9O_4$ (1466.35): calcd. C 71.3, H 7.37, N 8.60; found C 69.7, H 7.25, N 8.37. IR (KBr): $\tilde{\nu}$ = 3238 (N–H); 2253, 2143 (C≡N); 1625, 1614 (C=N); 1304, 1290 (C–O); 736, 729, 707 (Ar–H). χ_{dia} = -11.30×10^{-9} $m^3 mol^{-1}$.

Trinuclear Complex [Fe^{III}(salpet){$Fe^{II}(CN)_5(NO)$}Fe^{III}(salpet)]·$0.5CH_3OH \cdot 3.75H_2O$ (3a): Methanol solution of [Fe(salpet)Cl] (40 mL, 1 mmol, 5% excess) was combined with a methanol/water solution of $Na_2[Fe(CN)_5(NO)] \cdot 2H_2O$ (0.5 mmol in 5 mL of CH_3OH/H_2O, 1:1). In short time the color turned to violet-blue. The mixture was stirred for 1 h at 50 °C and then left to evaporate spontaneously for several days at room temperature. Dark-violet crystals were separated by filtration. Yield: 0.45 g (90%). $C_{43}H_{50}Fe_3N_{12}O_9$ (1046.13): calcd. C 49.4, H 4.78, N 16.1; found C 50.9, H 4.63, N 14.4. IR (KBr): $\tilde{\nu}$ = 3197 (N–H); 1630, 1616, 1596 (C=N); 2181, 2158, 2142 (split, C≡N); 1939, 1923 (N=O). UV/Vis (nujol): $\tilde{\nu}$ = 18000. χ_{dia} = -6.84×10^{-9} $m^3 mol^{-1}$.

Trinuclear Complex *trans*-[Fe^{III}(MeBu-salpet){$Ni(CN)_4$}Fe^{III}(MeBu-salpet)]·$2CH_3OH$ (3b): To a methanol/acetonitrile solution (1:1, 100 mL) of [Fe(MeBu-salpet)Cl] (0.72 mmol) K_2[$Ni(CN)_4$]·H_2O (0.35 mmol) was added and the suspension was stirred for 3 h at 60 °C. Resulting solution was filtered off and left to evaporate spontaneously. After 2 d black crystals of good quality were formed and these were separated by filtration, washed with cold methanol and ethyl ether. Yield: 0.39 g (86%). $C_{64}H_{90}Fe_2N_{10}NiO_6$ (1265.85): calcd. C 60.7, H 7.17, N 11.1; found C 60.3, H 7.04, N 11.3. IR (KBr): $\tilde{\nu}$ = 3670, 3315 (O–H); 3221 (N–H); 2128 (C≡N); 1628 (C=N); 1302 (C–O). χ_{dia} = -9.31×10^{-9} $m^3 mol^{-1}$.

Elemental analysis for cyanide-containing samples often gave a lower content for carbon and nitrogen; this effect is attributed to formation of stable carbides and nitrides, not accounted by chromatographic separation, when the cyanides burn in a flame of the commercial analyzer (FlashEA 1112, ThermoFinnigan).

Structure Determination: Single-crystal X-ray diffraction experiments were conducted by using a Gemini R CCD apparatus (Oxford Diffraction). Data reduction and empirical absorption correction were performed by CrysAlisRed or Bruker AXS programs.[10a,10b] The structures were solved by direct methods and refined by full-matrix least-squares procedure with the SHELX-97 program package.[10c] The X-ray crystallographic data are collected in Table 3. CCDC-700985 (for **1a**), -700986 (for **1b**), -700987 (for **1c**), -700988 (for **2a**), -700989 (for **2b**), -700990 (for **3a**), and -700991 (for **3b**) contain the supplementary crystallographic data for this paper. These data can be obtained free of charge from The Cambridge Crystallographic Data Centre via www.ccdc.cam.ac.uk/data_request/cif.

Physical Measurements: IR spectra were measured as KBr pellets (Magna FTIR 750, Nicolet) in the 4000–400 cm^{-1} region. Electronic spectra were measured by using the DRIFT method (Magna FTIR 750 Nicolet) in the region 5000–11000 cm^{-1} and in nujol mull (Specord 200, Analytical Jena) in the range 10000–50000 cm^{-1}. A conventional spectrometer was used in scanning the Mössbauer spectra at liquid helium and room temperature (^{57}Co/Rh source, calibration at α-Fe at room temperature). Magnetic susceptibility and magnetization measurements were done by using a SQUID magnetometer (Quantum Design) from 2 K at B = 0.1 T. The magnetization data were taken at T = 2.0 and 4.6 K, respectively. Raw susceptibility data were corrected for underlying diamagnetism by using the set of Pascal constants. The effective magnetic moment was calculated as usual: $\mu_{eff}/\ \mu_B = 798(\chi' T)^{1/2}$ when SI units are employed.

Table 3. Summary of X-ray crystallographic data.

	1a, 293 K	**1b**, 293 K	**1c**, 293 K	**2a**, 293 K
Formula	[Fe(salpet)Cl]	[Fe(MeBu-salpet)Cl]	[Fe(salpet)CN]·CH_3OH	[Fe(salpet){CN}Fe(salpet)]ClO_4·$2H_2O$
Composition	$C_{19}H_{21}N_3O_2FeCl$	$C_{29}H_{41}ClN_3O_2Fe$	$C_{21}H_{25}N_4O_3Fe$	$C_{39}H_{42}N_7O_{10}Fe_2Cl$
Formula weight	414.69	554.95	437.30	915.67
Crystal system	monoclinic	monoclinic	monoclinic	triclinic
Space group	$P2_1/c$	$P2_1/c$	$P2_1/c$	$P\bar{1}$
a [Å]	11.048(9)	16.385(3)	9.336(2)	11.515(2)
b [Å]	12.020(1)	10.993(2)	12.406(3)	12.160(2)
c [Å]	14.263(1)	16.849(3)	17.589(4)	15.170(3)
α [°]	90	90	90	82.85(3)
β [°]	108.34(7)	104.67(3)	100.74(3)	79.69(3)
γ [°]	90	90	90	76.75(3)
V [Å^3]	1797.8(3)	2935.9(10)	2001.5(8)	2026.5(6)
Z	4	4	4	2
$D_{calcd.}$ [g cm^{-3}]	1.532	1.256	1.451	1.507
Abs. coeff. [mm^{-1}]	1.006	0.634	0.784	0.849
F(000)	860	1180	916	956
Reflections collected	3651, 0.0531	7266, 0.0225	4056, 0.0205	8235, 0.0550
Refinement method	Full matrix least-squares on F^2			
Data/restraints/parameters	3651/0/239	7272/0/325	4056/0/264	8239/66/542
Final R indices, R_1	0.0474	0.0309	0.0322	0.0547
wR_2	0.1110	0.0776	0.0903	0.1341

Compound	**2b**, 90 K	**3a**, 293 K	**3b**, 293 K
Formula	[Fe(MeBu-salpet){CN}Fe(MeBu-salpet)](BPh_4)·$2CH_3CN$	[Fe(salpet){Fe($CN)_5$NO}Fe(salpet)]·$0.5CH_3OH$·$3.75H_2O$	[Fe(MeBu-salpet){Ni($CN)_4$}-Fe(MeBu-salpet)]·$2CH_3OH$
Composition	$C_{87}H_{108}BN_9O_4Fe_2$	$C_{43.5}H_{51.5}N_{12}O_{9.25}Fe_3$	$C_{64}H_{90}N_{10}O_6NiFe_2$
Formula weight	1466.35	1058.02	1265.846
Crystal system	monoclinic	monoclinic	monoclinic
Space group	$C2/c$	$C2/c$	$P2_1/n$
a [Å]	24.808 (3)	32.016 (6)	15.449 (3)
b [Å]	15.277 (2)	9.702 (2)	10.256 (2)
c [Å]	21.210 (2)	31.388 (6)	21.683 (4)
α [°]	90	90	90
β [°]	90.093 (3)	99.87 (3)	102.46 (3)
γ [°]	90	90	90
V [Å^3]	8038.7 (15)	9605 (3)	3354.6 (12)
Z	4	2	2
$D_{calcd.}$ [g cm^{-3}]	1.212	1.463	1.253
Abs. coeff. [mm^{-1}]	0.416	0.961	0.759
F(000)	3128	4388	1344
Reflections collected	8222, 0.0482	9402, 0.0529	6817, 0.0199
Refinement method	Full matrix least-squares on F^2		
Data/restraints/parameters	8222/0/474	9402/13/622	6817/1/383
Final R indices, R_1	0.0343	0.0465	0.0336
wR_2	0.0822	0.1207	0.0720

Supporting Information (see footnote on the first page of this article): Table of Mössbauer parameters, deconvoluted Mössbauer spectra.

Acknowledgments

Grant Agencies and project sponsors are acknowledged for their financial support: Research and Development Agency (Slovakia) (APVV 0006-07, COST-0006-06, VVCE 0004-07), VEGA (Slovakia) (1/0213/08), Deutscher Akademischer Austauschdienst (Germany), Deutsche Forschungsgemeinschaft (Germany) (RE-1627/1-3), Leibniz University (ZFM), Stefanik (France/Slovakia), Structural Funds (EU), Interreg IIIA.

[1] a) H. A. Goodwin, *Coord. Chem. Rev.* **1976**, *18*, 293; b) P. Gütlich, *Struct. Bonding (Berlin)* **1981**, *44*, 83; c) E. König, *Struct. Bonding (Berlin)* **1991**, *76*, 51; d) P. Gütlich, A. Hauser, H. Spiering, *Angew. Chem.* **1994**, *106*, 2109; e) P. Gütlich, Y. Garcia, H. A. Goodwin, *Chem. Soc. Rev.* **2000**, *29*, 419; f) A. Hauser, J. Jeftic, H. Romstedt, R. Hinek, H. Spering, *Coord. Chem. Rev.* **1999**, *190–192*, 471; g) P. Gütlich, H. A. Goodwin (Eds.), *Topics in Current Chemistry Vols. 233–235: Spin Crossover in Transition Metal Compounds I–III*, Springer, Berlin, **2004**.

[2] S. Zein, S. A. Borshch, *J. Am. Chem. Soc.* **2005**, *127*, 16197.

[3] a) J. A. Real, J. Zarembowitch, O. Kahn, X. Solans, *Inorg. Chem.* **1987**, *26*, 2939; b) J. A. Real, H. Bolvin, A. Bousseksou, A. Dworkin, O. Kahn, F. Varret, J. Zarembowitch, *J. Am.*

Chem. Soc. **1992**, *114*, 4650; c) J. A. Real, I. Castro, A. Bousseksou, M. Verdaguer, R. Burriel, M. Castro, J. Linares, F. Varret, *Inorg. Chem.* **1977**, *36*, 455; d) S. Brooker, P. G. Plieger, B. Moubaraki, K. S. Murray, *Angew. Chem. Int. Ed.* **1999**, *38*, 408; e) V. Ksenofontov, A. B. Gaspar, J. A. Real, P. Gütlich, *J. Phys. Chem. B* **2001**, *105*, 12266; f) V. Ksenofontov, H. Spiering, S. Reiman, Y. Garcia, A. B. Gaspar, N. Moliner, J. A. Real, P. Gütlich, *Chem. Phys. Lett.* **2001**, *348*, 381; g) A. B. Gaspar, V. Ksenofontov, M. Seredyuk, P. Gütlich, *Coord. Chem. Rev.* **2005**, *249*, 2661; h) A. B. Gaspar, M. C. Munoz, J. A. Real, *J. Mater. Chem.* **2006**, *16*, 2522; i) N. Suemura, M. Ohama, S. Kaizaki, *Chem. Commun.* **2001**, 1538; j) B. A. Leita, B. Moubaraki, K. S. Murray, J. P. Smith, J. D. Cashion, *Chem. Commun.* **2004**, 156.

[4] I. Nemec, R. Boča, M. Gembicky, L. Dlháň, R. Herchel, F. Renz, *Inorg. Chim. Acta*, submitted.

[5] a) O. Kahn, *Molecular Magnetism*, VCH, New York, **1993**; b) R. Boča, *Theoretical Foundations of Molecular Magnetism*, Elsevier, Amsterdam, **1999**.

[6] a) E. M. Holt, S. L. Holt, M. Vlasse, *Cryst. Struct. Commun.* **1979**, *8*, 645; b) G. Rogez, A. Marvilliers, P. Sarr, S. Parsons, S. J. Teat, L. Ricard, T. Mallah, *Chem. Commun.* **2002**, 1460.

[7] a) A. Bousseksou, F. Varret, J. Nasser, *J. Phys. I.* **1993**, *3*, 1463; b) R. Boča, Y. Fukuda, M. Gembický, R. Herchel, R. Jaroščiak, W. Linert, F. Renz, J. Yuzurihara, *Chem. Phys. Lett.* **2000**, *325*, 411; c) R. Herchel, R. Boča, M. Gembický, J. Kožíšek, F. Renz, *Inorg. Chem.* **2004**, *43*, 4103.

[8] K. Kaji, M. Sorai, A. J. Conti, D. N. Hendrickson, *J. Phys. Chem. Solids* **1993**, *54*, 1621.

[9] R. Boča, *Coord. Chem. Rev.* **2004**, *248*, 757.

[10] a) Oxford Diffraction Ltd, *CrysAlis CCD* and *CrysAlis RED* Abingdon, Oxfordshire, England, **2006**; b) Bruker AXS Inc., *APEX2*, *SMART-Plus* and *SADABS*, Madison, Wisconsin, USA, **2004**; c) G. M. Sheldrick, *Acta Crystallogr., Sect. A* **2008**, *64*, 112.

Received: February 18, 2009
Published Online: June 17, 2009

